Phys. Biol. 8 (2011) 026004 (14pp) doi:10.1088/1478-3975/8/2/026004

Self-organized models of selectivity in calcium channels

Janhavi Giri[1,2], James E Fonseca[1], Dezső Boda[3,4], Douglas Henderson[4] and Bob Eisenberg[1,5]

[1] Department of Molecular Biophysics and Physiology, Rush University, Chicago, IL 60612, USA
[2] Department of Bioengineering, University of Illinois at Chicago, Chicago, IL 60607, USA
[3] Department of Physical Chemistry, University of Pannonia, PO Box 158, H-8201 Veszprém, Hungary
[4] Department of Chemistry and Biochemistry, Brigham Young University, Provo, UT 84602, USA

E-mail: beisenbe@rush.edu

Received 16 July 2010
Accepted for publication 24 November 2010
Published 24 January 2011
Online at stacks.iop.org/PhysBio/8/026004

Abstract

The role of flexibility in the selectivity of calcium channels is studied using a simple model with two parameters that accounts for the selectivity of calcium (and sodium) channels in many ionic solutions of different compositions and concentrations using two parameters with unchanging values. We compare the distribution of side chains (oxygens) and cations (Na^+ and Ca^{2+}) and integrated quantities. We compare the occupancies of cations Ca^{2+}/Na^+ and linearized conductance of Na^+. The distributions show a strong dependence on the locations of fixed side chains and the flexibility of the side chains. Holding the side chains fixed at certain predetermined locations in the selectivity filter distorts the distribution of Ca^{2+} and Na^+ in the selectivity filter. However, integrated quantities—occupancy and normalized conductance—are much less sensitive. Our results show that some flexibility of side chains is necessary to avoid obstruction of the ionic pathway by oxygen ions in 'unfortunate' fixed positions. When oxygen ions are mobile, they adjust 'automatically' and move 'out of the way', so they can accommodate the permeable cations in the selectivity filter. Structure is the computed consequence of the forces in this model. The structures are self-organized, at their free energy minimum. The relationship of ions and side chains varies with an ionic solution. Monte Carlo simulations are particularly well suited to compute induced-fit, self-organized structures because the simulations yield an ensemble of structures near their free energy minimum. The exact location and mobility of oxygen ions has little effect on the selectivity behavior of calcium channels. Seemingly, nature has chosen a robust mechanism to control selectivity in calcium channels: the first-order determinant of selectivity is the density of charge in the selectivity filter. The density is determined by filter volume along with the charge and excluded volume of structural ions confined within it. Flexibility seems a second-order determinant. These results justify our original assumption that the important factor in Ca^{2+} versus Na^+ selectivity is the density of oxygen ions in the selectivity filter along with (charge) polarization (i.e. dielectric properties). The assumption of maximum mobility of oxygens seems to be an excellent approximate working hypothesis in the absence of exact structural information. These conclusions, of course, apply to what we study here. Flexibility and fine structural details may have an important role in other properties of calcium channels that are not studied in this paper. They surely have important roles in other channels, enzymes, and proteins.

1. Introduction

Selectivity arises from the interactions of the ions and side chains of proteins constrained by the geometry and properties

[5] Author to whom any correspondence should be addressed.

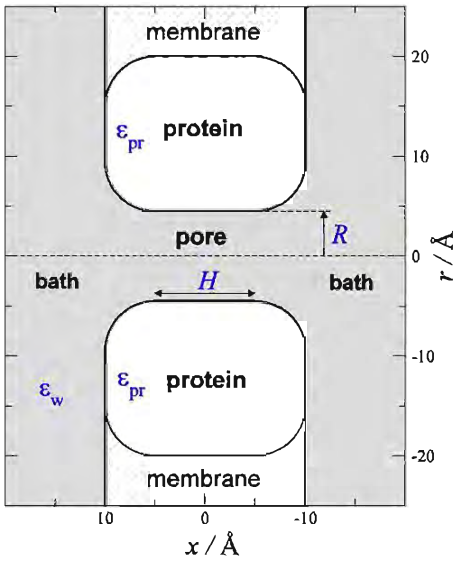

Figure 1. Geometry of the model of the ion channel. The parameters $R = 3.5$ Å, $H = 10$ Å, and $\varepsilon_{pr} = 10$ are used in the simulations in this paper. In the figure, 'x' corresponds to the distance z.

of the rest of the protein, and the surrounding bathing solutions. For a long time—as long as the issue of selectivity has been considered by biologists—we have believed that selectivity depends on the detailed structure of the binding sites for ions. Selectivity has been thought to depend on the exact atomic arrangements of side chains, ions, and other nearby molecules [1, 2]. The selectivity of the calcium channel we consider here is particularly important because of the enormous importance of the channel [3–21]. The L-type calcium channel that we have in mind controls the contraction of the heart and signaling in skeletal muscle. Few channels are more important than the calcium channel because calcium concentration inside cells is used as a signal in almost every tissue of an animal.

It has come as a surprise that a model of selectivity that includes only a few features of the atomic structure has been able to describe the selectivity properties of calcium and sodium channels very well, in all solutions over a wide range of conditions, with only two adjustable parameters using crystal radii of ions [22, 23]. This model is skeletal in its simplicity, representing side chains as charged spheres unrestrained by connections to the surrounding protein. This model represents the selectivity filter of calcium and sodium channels as cylinders containing spherical structural ions (modeling the terminal groups of side chains) free to move within the cylinder but unable to leave it (figure 1). Note that water is present in this model only as a dielectric; the primitive implicit solvent [24–48] model of ionic solutions is used and extended into the channel. The *question* is how can this simple model possibly work, given that it includes no detail of the protein structure and uses only a crude representation (to put it kindly) of the side chains and their interaction with ions.

The *answer* we give is that the model works because it captures the features of the binding sites of calcium and sodium channels that biology actually uses to produce selectivity. Many other physical phenomena could be used to produce selectivity, and probably are in other types of channels, transporters, enzymes, and proteins, let alone physical systems in general. It seems here however that biology has used only the simplest, the competition between electrostatic forces and volume exclusion in very concentrated systems of ions and side chains.

The two cations Ca^{2+} and Na^{+} that compete for the channel arrive from a bath of a given composition and mix with the side chains of the channel protein in our model. The winner of the competition is the ionic species whose binding minimizes the free energy $F = U - TS$. Electrostatic attraction between the side chains and the cations decreases the energy U, while competition for space in the crowded selectivity filter chiefly influences the $-TS$ term. The entropic term is most directly influenced by the flexibility of side chains. Indirectly, of course, everything is influenced by everything. The U and $-TS$ terms are not uncoupled, of course [49], but separating U and $-TS$ terms provides a useful framework to understand selectivity.

Our model assumes a large mobility (flexibility) of the terminal groups (eight half-charged oxygen ions, in this paper) of side chains. In reality, the movement of side chains is restricted because they are tethered to the polypeptide backbone of a protein. The side chains of acidic and basic residues in real proteins are not fully rigid (though they are not entirely mobile either) and have considerable mobility during thermal motion.

The goal of this paper is to study the effect of the flexibility of the side chains on physical quantities computed by Monte Carlo (MC) simulation. The basic quantities computed by the simulation are the profiles of spatial distribution of the various ionic species. These distributions, as expected, are very sensitive to restrictions in the mobility of oxygen ions.

Integration of the ionic profiles provides quantities comparable to experiments. These integral properties characterize selectivity from two profoundly different points of view.

(1) The integral of the ionic profile (of a given species) itself over a given volume (of the selectivity filter, for example) describes the *binding affinity* of the given ionic species to this volume. This quantity—that we call 'occupancy'—is proportional to the probability that a given ionic species binds to the selectivity filter in competition with other kinds of ions. Occupancy is a result of minimized free energy, an equilibrium concept, but occupancy exists in non-equilibrium systems as well, of course. It must be computed by a different theory in that case, one that includes nonequilibrium parameters (like conductance) and spatially nonuniform boundary conditions [50, 51].

(2) The resistance of the channel is the sum of the resistance of a series of (infinitesimally thin) disks, as described precisely later in the Methods section. Resistance is a more dynamic variable than occupancy. Each disk has resistance determined by the amount and mobility of the ions in the disk. The amount is proportional to the reciprocal of the concentration of ions, times the volume of the disk. The sum is actually the integral of the reciprocal of the profile of ionic concentration

over a length of the ionic pathway. The integral is proportional to the resistance of that length to the current of the ionic species in question. This resistance describes the selectivity of ion channels directly measurable from measurements of current or flux through channels under near equilibrium conditions. It is more sensitive to local variations in the ionic profiles than occupancy. It is expected, therefore, that conductance is more sensitive to variations in flexibility of side chains too.

We will change the flexibility of the oxygen ions in different ways and analyze how the physical quantities mentioned above change as flexibility is changed. We obtain quite different behavior for the profiles, occupancies, and conductances as a function of varying flexibility.

An important result of analysis of this model is that the locations of ions and side chains have a 'self-adjusting' nature as ion concentrations are changed in the bath, or the nature of the side chains is altered, for example, from EEEE to EEEA in a calcium channel or DEKA to DEEA in a sodium channel. Side chains are mobile in our model and so they change their distribution as parameters of the model change. In this picture, the structure of the binding site is a computed consequence of thermodynamic and geometrical constraints and all the forces present in the system. Thus, by *'structure'* we mean the equilibrium profiles of spatial distribution of the concentration of all the ions obtained as ensemble averages of converged simulations. This structure obviously changes as experimental conditions change.

The sensitivity of the structure to the location and flexibility of side chains helps answer the general paradox: 'How can a model without a detailed structure account for complicated properties of two different types of channels under so many conditions?' The answer to the question is that the model computes the structure. The channel structure is different in different conditions because of the sensitivity of spatial distributions. Thus, biological properties that are sensitive to structure will be sensitive to location and flexibility of side chains. Integrated properties like conductance are not so sensitive.

In other words, the model of selectivity is an induced-fit model, in which the structure of the binding site is induced by all the forces in the system, depending on the ion concentrations in the bath and the other parameters of the problem. The fit of the side chains to the ions is induced by the minimization of the free energies of the system. The model is a self-organized model. In our model, the only energies that determine the structure are electrostatic and excluded volume. No energies with a more chemical flavor are included in the present version of the model.

Unfortunately, we do not know anything about the actual locations of side chains in real calcium and sodium channels because x-ray structures are unavailable. It is possible to hypothesize the locations assuming various homologies with the known structure of the KcsA potassium channel [52, 53]. We followed a different route as described in the Model section.

We conclude that ionic distribution profiles are sensitive functions of locations of immobilized side chains and their flexibility. Occupancy, on the other hand, is less sensitive to flexibility because its first-order determinant is the density of ions in the selectivity filter as we established earlier [54, 55]. Conductance, the most interesting quantity of the three, lies in between because it depends on both occupancy (the number of available charge carriers) and fine details in the distribution profiles. The conductance of a single channel of fixed diameter depends on the sum of many differential 'resistors' because it measures the 'series resistance' of the single channel. The conductance depends on the reciprocal of the concentration for this reason and is very sensitive to high resistance obstructions in the permeation pathway even if they occur over a tiny length. These high resistances are produced by the low concentrations of mobile ions in the depletion zones in the ionic profiles [56]. Depletion zones are responsible for many of the most important properties of transistors [57–59]. Transistors and channels involve quite similar physics and are described by quite similar equations, but the charge carriers of transistors are points with no size.

If three-dimensional structures for calcium and sodium channels become available, the information gained must be built into our model. Until then, our approach—that allows the side chains to find their optimal distribution automatically in the simulation—seems to be a good way to proceed. It allows us to construct a functional skeletal model that fits a wide range of data from two channel types under many conditions with only two parameters. It makes understanding of permeation and selectivity mechanisms of real calcium and sodium channels possible, if permeation and selectivity are viewed as outputs of that simplified model.

2. Methods

2.1. Model of channel and electrolyte

We use a reduced model to represent the L-type calcium channel because a crystallographic structure is not available. We know from the experimental literature that Ca^{2+} selectivity in this channel is determined and regulated by the four glutamates of the pore-lining loops which form the selectivity filter [60–63]. The negatively charged carboxyl (COO^-) side chains of these glutamates extend into the selectivity filter region of the channel [64]. As Sather and McCleskey put it in their review [63] 'The calcium channel field is convinced that the EEEE carboxyl side chains project into the pore lumen' to form a mixture of ions and side chains that has been called an 'electrical stew' [65].

At room temperature of 300 K, these side chains as well as the surrounding cations interact and exhibit thermal motions. The four glutamates (EEEE) contribute to a fixed charge of $-4e$ on the selectivity filter. This existing information about the L-type calcium channel is used to build a reduced model [55, 66].

In our reduced model the channel is represented as a doughnut-shaped object with a pore in the middle connecting the two baths (figure 1). The protein which forms the pore is represented as a continuum solid with dielectric coefficient, $\varepsilon_p = 10$. The central, cylindrical part of the pore, the

selectivity filter, is assigned a radius $R = 3.5$ Å and length $H = 10$ Å. The model is rotationally symmetric along the pore axis. The selectivity filter (−5 Å, 5 Å) contains the negatively charged side chains extending from the polypeptide backbone of the channel protein into the pathway for ionic movement. We represent the carboxyl (COO^-) side chains as a pair of negative half charged oxygen ions ($O^{1/2-}$) resulting in eight oxygen ions (also called 'structural ions'). The net charge in the selectivity filter therefore sums to $-4e$. The side chains are free to rearrange inside the selectivity filter of the channel but cannot leave the selectivity filter. The mobile ions (Na^+, Ca^{2+}, Cl^-) as well as the oxygen ions of the carboxyl groups are hard spheres and are assigned Pauling crystal radii (see the caption to figure 1). The structural ions mix with the mobile ions producing a flexible but confined environment in the selectivity filter. The structural ions have different degrees of flexibility as described later. Water is represented implicitly as a dielectric ($\varepsilon_w = 80$).

The simulation cell is a cylindrical compartment that is kept small to save computation time. The simulation cell is checked to be sure that it is large enough that our final results do not depend on its size. The dimensions of the simulation cell are chosen depending on the ionic concentrations in the surrounding bath solutions. The baths are separated by a lipid membrane 20 Å thick except where the channel protein is found. Ions are excluded from the lipid membrane. The filter is assumed to have a dielectric coefficient of 80. If more realistic values were used, the amount of computation required for the electrostatics increased and no significant effects were noted on the simulation results [66, 67].

2.2. *Method: equilibrium grand canonical MC simulations*

We perform MC simulations using Metropolis sampling in the grand canonical ensemble [68] which allows us to efficiently simulate the very small ionic concentrations important for calcium channels. The details of the methods of sampling and their acceptance tests have been described in [67–70] and earlier papers. We simulate an equilibrium grand canonical ensemble at room temperature 300 K. The chemical potentials of ions are the inputs chosen for the grand canonical ensemble and are determined separately using an iterative method [71, 72]. The acceptance tests of new particle configurations involve the total electrostatic energy of a configuration. The net electrostatic energy of the system includes the Coulombic interactions between the ions and the side chains and the interactions resulting from the charges induced at dielectric boundaries which are computed using the induced-charge computation method [73]. The GCMC simulations that we present in the Results section are averages of many runs performed on multiple processors and beginning from different seed configurations. Each result is the average of 6×10^8 to 1.2×10^9 MC configurations.

2.3. *Simulated experimental setup*

The micromolar block of Na^+ current observed by McCleskey *et al* [9, 74] is a characteristic behavior of the L-type calcium channel. In this experiment, $CaCl_2$ is gradually added to a fixed background of 30 mM NaCl. The experiments show that 1 μM of Ca^{2+} reduces the current through the L-type calcium channel to the half its value in the absence of Ca^{2+}. This result implies that the selectivity filter of the calcium channel contains a high affinity binding site for cations, especially for Ca^{2+}. The strongly bound Ca^{2+} obstructs the diffusion of Na^+ ions in the packed and narrow selectivity filter. This experiment was the main target of several theoretical and simulation studies of the L-type calcium channel [23, 54, 66, 67, 70, 75, 76].

As far as we know, our reduced model is the only one that is able to produce this strong Ca^{2+} versus Na^+ selectivity in a range of conditions. Indeed, most computations of selectivity do not contain concentration as a variable at all [1, 2, 77]. Moreover, the classical kinetic models of selectivity [78, 79] assume the energy landscape or the barrier to be independent of ionic concentrations which is an implausible approximation given the ubiquity of shielding in ionic solutions and the reality of Gauss' law. These and other difficulties with classical models have been evident for a long time [80–90]. Indeed, the 'law' of mass action itself has recently been shown [101] to apply only to infinitely dilute solutions of noninteracting particles, if it is used with constant rate constants as in the classical models of channels [78, 79].

Our simulations (analyzed with the integrated Nernst–Planck equation, see later equation (3)) show that at 1 μM Ca^{2+} the average number of Na^+ ions in the selectivity filter drops to half the value it has at zero Ca^{2+}. Under those conditions, Ca^{2+} ions occupy the central binding site in the filter, but they do not contribute to the current because of the depletion zones formed at the entrances of the filter [23, 76]. This mechanism is in agreement with an earlier intuitive description of the mechanism of this block [91].

Some simulations were carried out for the entire range of Ca^{2+} concentrations as used by Almers and McCleskey in their experiment (from 0 to 10^{-2} M). Others were just carried out for the special case when $[Ca^{2+}]$ is 1 μM. In experiments, the replacement of Na^+ by Ca^{2+} takes place in a narrow concentration range around this value.

2.4. *Models of flexibility*

There are two limiting cases of the flexibility of side chains.

(1) The 'flexible case' is our usual model with maximum flexibility. In this case, oxygen ions are perfectly mobile inside the selectivity filter but they are confined within the filter by hard walls. In this model, oxygen ions automatically find their average distribution that minimizes free energy of the system. As cations (Na^+ or Ca^{2+}) enter the filter, oxygen ions rearrange and make it possible for the cations to pass the channel [56]. The distribution of the oxygens is an output of the simulation.

There is agreement [60, 61, 63, 92, 93] that side chains in the filter of calcium channels are quite flexible. They are in constant thermal motion and the long (three-carbon) chains allow the COO^- terminal groups considerable freedom to move within the channel. Nonetheless, the maximum mobility case obviously overestimates the flexibility of side chains.

(2) The 'fixed case' places oxygen ions in fixed positions and allows zero mobility. This assumption roughly corresponds to the system at 0 K and underestimates the flexibility of side chains.

Unfortunately, the x-ray structure for the calcium channel is not yet known. Therefore, instead of assuming the initial positions of the oxygens, we choose certain fixed oxygen configurations from the billions of possible configurations that are computed during an MC simulation of the '*flexible*' case. The nature of MC simulations ensures that all these configurations occur in the sample in a Boltzmann distribution [94, 95]. Each configuration we choose as a fixed configuration is one of the configurations of the equilibrated system. In other words, they can be called '*probable*' configurations.

In this paper, we chose configurations that are even 'more probable' using a criteria based on electrostatic energy. We determine those configurations by carrying out the usual MC simulation for 50 blocks where each block consists of 5×10^5 trials. After a block is finished, we displace the oxygen ions to ensure that the next block samples new configurations. After every MC trial in each block we calculate the electrostatic interaction energy of the oxygen ions with every other ion. A running average of this energy is updated. At the end of each block, the instantaneous locations of the oxygen ions and the corresponding running averages of the energy for that block are saved. Therefore, at the end of the simulation for each of the 50 blocks we obtain a set consisting of locations for the eight oxygen ions which represent the instantaneous configurations at the end of the block and the corresponding average energy of that block. We have chosen 10 configurations of the oxygens from these 50 configurations that have the lowest average energy and we call them the '*low energy*' configurations. We have performed simulations for these cases in the usual way except that MC movements were not performed for the oxygen ions. We performed simulations for $[CaCl_2] = 10^{-6}$ M and $[CaCl_2] = 0$ M so we can relate our results for 10^{-6} M to results in the entire absence of Ca^{2+}.

In addition to these ten '*fixed low energy*' configurations, we chose a configuration of oxygens that had the lowest energy in the sample we checked. This configuration does not have the lowest energy in general; it just has the lowest energy in the 50 configurations of oxygens we examined in our simulation. We will call this case the '*lowest energy*' case. We simulated the lowest energy case for concentrations spanning the whole Ca^{2+} concentration range used in experiments.

Because we do not know the exact structure of the selectivity filter, the configurations just defined were not selected with the purpose to mimic any realistic structure. They were chosen to study the effect of fixing the oxygens somewhere. A large number—hundreds—of other configurations were chosen by ad hoc methods in the course of these calculations, as we developed our procedures. From all this work, we are quite certain that the conclusions that we draw from the results are quite general and independent of the actual positions of the oxygen ions. The qualitative conclusions of our work are not sensitive to the exact method of choosing the 'low energy' configurations. The exact configuration we call 'low energy' has little importance.

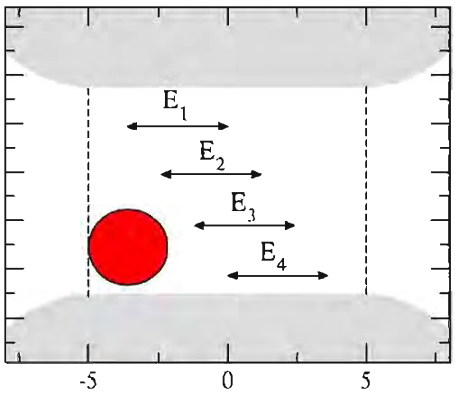

Figure 2. In the 'restricted' case, four pairs of oxygen ions are restricted to four overlapping regions in the selectivity filter along the z-axis of the pore. The ion centers are restricted to the following intervals: E_1: [−3.6, 0], E_2: [−2.4, 1.2], E_3: [−1.2, 2.4], and E_4: [0, 3.6]. The abscissa represents the distance along the channel axis in Å.

To study the effect of oxygen flexibility in more detail, we constructed models in which oxygen ions have partial flexibility. These models lie between the fixed and flexible cases defined above.

(1) *The 'restricted' case* restricts the four pairs of oxygen ions to stay in four narrow regions. We assume that the glutamate residues are not concentrated at one position of the selectivity filter, but rather they are distributed along the axis of the pore confined in cylinders defined by the filter wall and hard walls at fixed z-coordinates as shown in figure 2. The regions in which the oxygen pairs are confined overlap and they prevent a given pair to diffuse elsewhere in the filter. The distribution of oxygen ions is more uniform in this case than in the '*flexible*' case. We performed simulations for this case in the whole Ca^{2+} concentration range where the oxygen ions were perfectly mobile in the selectivity filter $|z| \leqslant 3.6$ Å.

(2) *The 'confined' case.* In this case, we start with the '*lowest energy fixed*' position of the oxygen ions and gradually allow them more and more mobility in the following way. We define spheres of radii R_{ox} around these fixed positions and allow the oxygen ions to move freely inside these spheres. The oxygen ions cannot leave these spheres. Then, we gradually increase the size of these spheres thus increasing the mobility of the oxygen ions. Any radius that is larger than about 7 Å effectively corresponds to the '*flexible*' case. Thus, we designed a scheme in which we smoothly change the model between the two limiting cases of flexible and fixed. We performed simulations in the confined case only for $[CaCl_2] = 10^{-6}$ M and $[CaCl_2] = 0$ M.

2.5. Pore conductance

We use the integrated Nernst–Planck formulation of Gillespie and Boda [76, 96] to relate the equilibrium GCMC simulation to the linearized slope conductance estimated in experiments with equal concentrations of ions on both sides of the

channel. The integrated Nernst–Planck formulation based on the resistors-in-series model is used to calculate the conductance of each ionic species in the pore region. The combination of the integrated Nernst–Planck equation (3) and MC simulations has been successful in reproducing the anomalous mole fraction effect in L-type calcium channel known from the experiment [76]. We reproduce here the key equations that we use in our calculations.

The ions are assumed to move diffusively and their current is described by the Nernst–Planck equation:

$$-\mathbf{J}_i(\mathbf{x}) = \frac{1}{k_B T} D_i(\mathbf{x}) \rho_i(\mathbf{x}) \nabla \mu_i(\mathbf{x}), \tag{1}$$

where $\mathbf{J}_i(\mathbf{x})$, D_i, ρ_i, and μ_i are the local flux density, diffusion coefficient, density and the electrochemical potential of ion species i, respectively. The value k_B is the Boltzmann constant and T is the temperature. We focus on the selectivity filter region of length L confining the structural ions. The chemical potential $\mu_i(z)$ and the diffusion coefficient $D_i(z)$ are assumed to be uniform over the cross-section of the selectivity filter. With these approximations, the total flux of ion species i through the pore:

$$-J_i^T = \frac{D_i}{k_B T} \frac{\mathrm{d}\mu_i(z)}{\mathrm{d}z} n_i(z), \tag{2}$$

where $n_i(z)$ is the axial number density of ions (number per unit pore length) at the axial location z.

The total conductance γ of the pore in the presence of symmetrical bath solutions at the end of the selectivity filter region containing several ion species of charge $z_i e_0$ and a very small voltage applied across the system is

$$\gamma = e_0 \sum_i z_i \frac{\partial J_i^T}{\partial V} |_{V_{L/2} - V_{-L/2}}$$

$$= \sum_i D_i \frac{z_i^2 e_0^2}{k_B T} \left(\int_{-L/2}^{L/2} \frac{\mathrm{d}z}{n_i(z)} \right)^{-1}. \tag{3}$$

Note that the conductance depends on the square of the charge of the ions $z_i^2 e_0^2$. The axial densities of ion species n_i are computed from the MC simulations. The diffusion coefficient of ions is an external parameter not determined by our simulation that must be provided as an input to our computation. We deal with normalized conductances, and therefore, it is sufficient to specify the ratio of diffusion coefficients of the two cations D_{Ca}/D_{Na}. We use the value $D_{Ca}/D_{Na} = 0.1$ in our computation. Dynamical MC (DMC) simulation [56] recently verified an early suggestion of Nonner and Eisenberg [75] that the diffusion coefficient of Ca^{2+} in the selectivity filter is much smaller than that of Na^+.

The approximations and equations used to calculate the pore conductance γ quantify the current through the channel. It is very important here to emphasize that the estimation of pore conductance requires only the spatial (i.e. cross sectional) uniformity of the chemical potential, which does not imply that the other variables, such as the spatial number density of the ions or the electrical potential, are spatially uniform. The concentration profiles used in these calculations are obtained from simulations performed under equilibrium conditions and with self-consistent electrostatics. When the system is off equilibrium the concentration profiles will have to be recomputed to be self-consistent as done in density functional/Poisson–Nernst–Planck theory [76, 96–100] or more recently with variational methods [50, 51, 101]. Thus, our conductance γ of equation (3) does not include the nonlinear effects that may occur when other voltages or concentration gradients are applied. The non-linear effects on the potential profiles cannot be determined by the equations given here. Non-linear effects are important in channels because channels are devices that use gradients of free energy to perform their function. Non-linear effects are responsible, for example, for the properties of semiconductor devices and those effects are not present near equilibrium where our conductance equation applies. Such effects can be computed by Poisson–Nernst–Planck equations if charge carriers have zero diameter or by a modification of those equations if the charge carriers have finite diameter [50, 51, 98, 101–103]. The slope conductance γ is nonetheless quite informative, because experiments show that current–voltage curves are often linear in a wide voltage range around equilibrium.

3. Results

We analyze our results on various levels of abstraction. The primary output of our simulations is concentration profiles. These profiles describe the probability of various ions being found in a given position, or, looking at the same thing from a more dynamical point of view, they describe the relative amount of time that these ions spend in a given location. We will show profiles averaged over the cross-section of the channel. We can derive two kinds of integrated quantities from the concentration profiles.

(1) The integral of the concentration profile provides the average number of the given ionic species in a certain sub-volume of the system. We will show the average number of ions integrated over the selectivity filter and we will call these numbers occupancies. The occupancies of Na^+ and Ca^{2+} describe equilibrium binding affinity of these ions to the selectivity filter.

(2) The other integrated quantity of interest is the integral of the reciprocal of the concentration profile based on the Nernst–Planck equation (see the Methods section, equation (3)). This integral is proportional to the resistance of the pore to a given ionic species in the region of validity of the equation. We will show conductance values γ that are the reciprocals of the resistances. We will concentrate on conductances of Na^+, because Ca^{2+} does not conduct significant current in the conditions of interest, at micromolar [$CaCl_2$].

We work with normalized conductances. Usually, we normalize with respect to the Na^+ conductance computed in the absence of Ca^{2+}. Because in this paper we compare different systems, we have two choices regarding how we normalize the conductance.

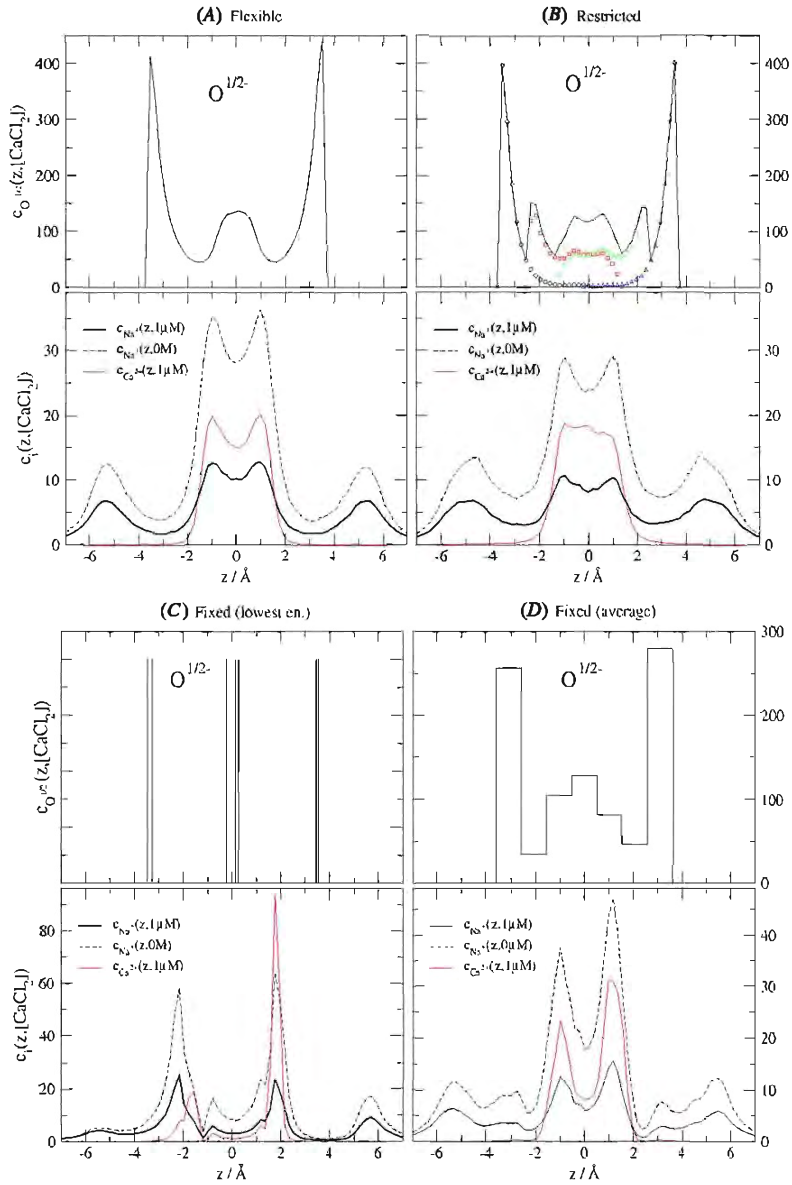

Figure 3. Concentration profiles for oxygen (top row) and free ions (bottom row) for three different restrictions of the oxygens. (*A*) 'Flexible' case: the oxygen ions are fully mobile inside the selectivity filter, but cannot leave it. (*B*) 'Restricted' case: four pairs of oxygens are restricted to four overlapping regions inside the selectivity filter as shown in figure 2. Profiles with different symbols and colors in the top panel in (*B*) refer to these four oxygen pairs. The solid black line is the sum of these four profiles. (*C*) 'Fixed' case: the eight oxygens are fixed in positions that correspond to the lowest-energy configuration of a finite sample. The vertical lines in the top panel in (*C*) represent Dirac deltas corresponding to these fixed positions. In the bottom row, we show the profiles for Na^+ at $[CaCl_2] = 0$ M (dashed black line) and $[CaCl_2] = 10^{-6}$ M (thick solid black line). The thin solid red line represents the Ca^{2+} profiles for $[CaCl_2] = 10^{-6}$ M. (*D*) 'Average' case is similar to (*C*), but represents the averages of the ten low energy configurations.

(a) First, each model ('*flexible*', '*restricted*', '*fixed*' or '*constrained*' cases) can be normalized by its own zero-Ca^{2+} conductance. Each model is normalized by itself. In this way, g is always normalized to 1 in the limit $[CaCl_2] \to 0$. This kind of normalization is used in the experimental literature [9, 60, 61, 63, 74, 93].

(b) To compare the absolute values of conductances computed from different models, we can normalize with respect to one fixed value in all cases. This way, we can draw conclusions about how changing the flexibility of the oxygen ions influences the ability of the channel to conduct Na^+. Correlations between the integrated quantities are shown by plotting one integrated quantity on the ordinate, and the other integrated quantity on the abscissa.

Figure 3 shows concentration profiles for the (*A*) '*flexible*', (*B*) '*restricted*', (*C*) '*lowest energy fixed*', and (*D*) the average of the ten '*low energy fixed*' cases. The oxygen

concentration profiles (top panels in figures 3(*A*)–(*D*)) are similar in the '*flexible*' and '*restricted*' cases: oxygen ions tend to accumulate at the entrances of the filter because the negative oxygen ions repel each other to the confining walls of their compartment. A third peak appears in the center of the filter in the '*flexible*' case because of packing. In the '*restricted*' case, the total oxygen profile is a sum of the four profiles for the four oxygen pairs. The '*restricted*' case has two additional peaks. The distribution of oxygens is more flat than in the '*flexible*' case. The vertical lines in the '*lowest energy fixed*' case represent the Dirac-delta function describing the positions of the fixed oxygens.

Each simulation performed with a given fixed oxygen configuration provides an adequate sampling of all possible configurations of the free ions (Na^+, Ca^{2+}, and Cl^-), because of the large number of configurations calculated (and examined) in each simulation. Many of the configurations we have chosen for the fixed oxygens produce the configurations of the free ions that resemble results of simulations of the totally '*flexible*' case. The ten selected '*low energy fixed*' simulations then correspond to a sample that resembles a sample of the '*flexible*' case. The resemblance is approximate because we have only ten '*low energy fixed*' oxygen configurations compared to the millions of oxygen configurations found in a usual simulation for the entire '*flexible*' case. (Remember the result of a MC simulation is a set of configurations, not a single configuration.) To test this idea, we averaged the concentration profiles obtained from the ten simulations for the ten '*low energy fixed*' cases. The oxygen profile shown in the top panel in figure 3(*D*) was calculated using a wide (1 Å) bin. The overall behavior of the curve is very similar to the oxygen profile for the '*flexible*' case despite the small (ten) sample for the oxygens in the '*low energy fixed*' case.

The bottom panels in figures 3(*A*)–(*D*) show the results for the free ions (Na^+ and Ca^{2+}) for $[CaCl_2] = 10^{-6}$ M and $[CaCl_2] = 0$ M. A micromolar amount of Ca^{2+} in the bath is sufficient to decrease the Na^+ concentration in the pore to half of its value in the absence of Ca^{2+}. (Compare the thick solid and thin dashed lines.) From this point of view, the four models behave similarly. The similarity is especially striking in the case of the '*lowest energy fixed*' oxygen configuration: although the details of the distribution of Na^+ ions are very different from those in the '*flexible*' and '*restricted*' cases, the relative behavior with respect to the zero Ca^{2+} curve is similar. This is also true for the average of the ten '*low energy fixed*' cases.

This is the first important conclusion of our paper: adding Ca^{2+} to the systems simply scales the Na^+ spatial profiles but it does not change the shape of the spatial distribution. Furthermore, adding 1 μM Ca^{2+} scales the Na^+ profiles similarly in the three different cases, thus producing similar selectivity behavior. This scaling is shown by figure 4, where we plot the ratio of the Na^+ concentration spatial profiles for $[CaCl_2] = 10^{-6}$ M and $[CaCl_2] = 0$ M. This ratio is similar for the three cases plotted showing that these three models have similar selectivity behavior. The ten '*low energy fixed*' cases have the same behavior on average. The shape of the curves is very similar in the individual cases too (data not shown).

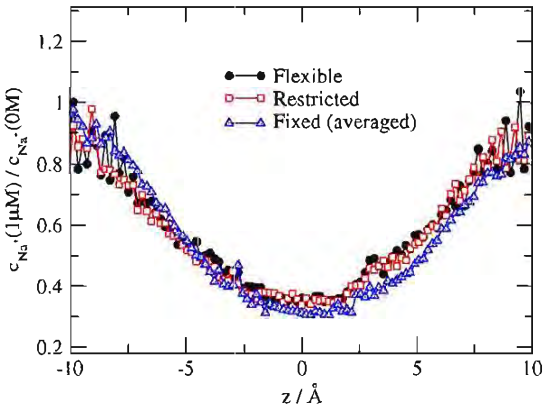

Figure 4. The ratio of the Na^+ concentration profiles for $[CaCl_2] = 10^{-6}$ M and 0 M for the three cases depicted in figure 3.

Ca^{2+} profiles also behave similarly in the various cases in this respect. As Ca^{2+} is added, it appears in the selectivity filter wherever space is available (at the minima of the oxygen profiles). The common feature is that Ca^{2+} is absent at the filter entrances ($3.0 \leqslant |z| \leqslant 5$ Å).

Depletion zones—here at the filter entrances—have the property that the reciprocal of the Ca^{2+} concentration is large at these locations, so the integral (of the reciprocal of the concentration profile, which is the resistance) is also large. Various slices of the channel along the pore axis behave as resistors connected in series. One high-resistance element makes the resistance of the whole circuit high. Therefore, Ca^{2+} does not carry any current at this concentration, it only blocks (reduces) the current of Na^+.

Here we see the origin of the most noted experimental property of the calcium channel, calcium block. Calcium block of sodium current is produced by the selective binding of Ca^{2+} in the selectivity filter. The absence of calcium current (an important part of the block) is produced by depletion zones. The depletion zones are computed outputs of our model, not assumed inputs.

To describe further the selectivity behavior of the channel models using the integrated quantities, we show titration curves. We plot these integrated quantities as a function of the concentration of added Ca^{2+}.

Figure 5(*A*) shows the occupancy curves for both Na^+ and Ca^{2+}. Ca^{2+} gradually replaces Na^+ in the filter as $[CaCl_2]$ increases. At about 1 μM, the two ions have equal amount in the filter. Also, at this Ca^{2+} concentration the amount of Na^+ drops to half in the filter. The three different cases behave similarly in spite of the differences in fine details in the concentration profiles (see figure 3).

Figure 5(*B*) shows the normalized Na^+ conductances (normalized by their own zero Ca^{2+} values) for the three different cases. The current carried by Na^+ is gradually decreased as Ca^{2+} is added in accordance with the experiment of Almers and McCleskey [9, 74]. As we demonstrated before, we reproduce the micromolar block of the current by Ca^{2+}, our curves agree well with the experimental curve in the low $[CaCl_2]$ range. Ca^{2+} starts to conduct at high $[CaCl_2]$. In this

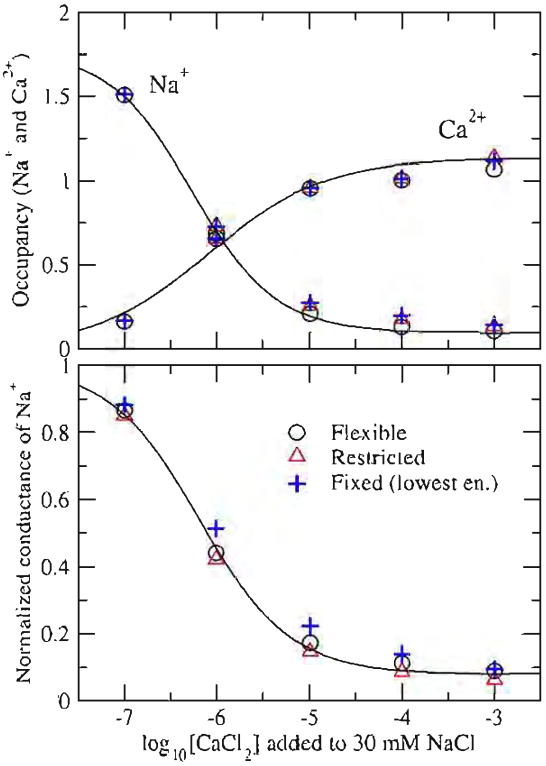

Figure 5. (*A*) The average number (occupancy) of Na^+ (decreasing curves) and Ca^{2+} (increasing curves) ions as functions of $\log_{10}$ [$CaCl_2$] for the three different cases depicted in figure 3. (*B*) The conductance of Na+ ions normalized by the conductance at [$CaCl_2$] = 0 M as a function of $\log_{10}$ [$CaCl_2$] for the three different cases.

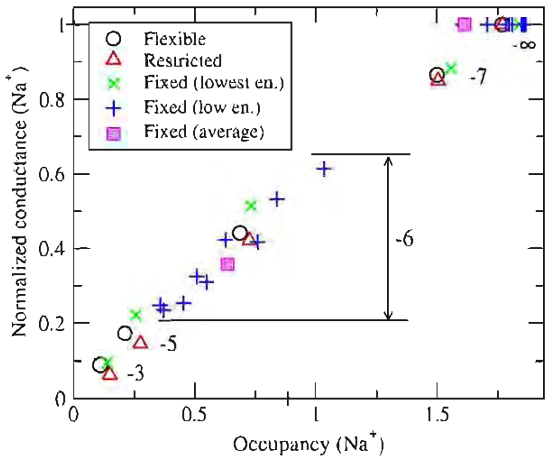

Figure 6. Normalized conductance of Na^+ versus occupancy of Na^+ in the selectivity filter at different $CaCl_2$ concentrations for the three different cases depicted in figure 3. The green × symbols represent results for the lowest-energy 'fixed' oxygen configuration used in figure 3. The blue + symbols represent results for ten selected 'fixed' oxygen configurations with low energies. The pink □ symbols represent averaged results for ten selected 'fixed' oxygen configurations with low energies. The numbers near the symbol denote the values of $\log_{10}$ [$CaCl_2$]. Na^+ conductance for a given case is normalized by the Na^+ conductance for that particular case in the absence of Ca^{2+}.

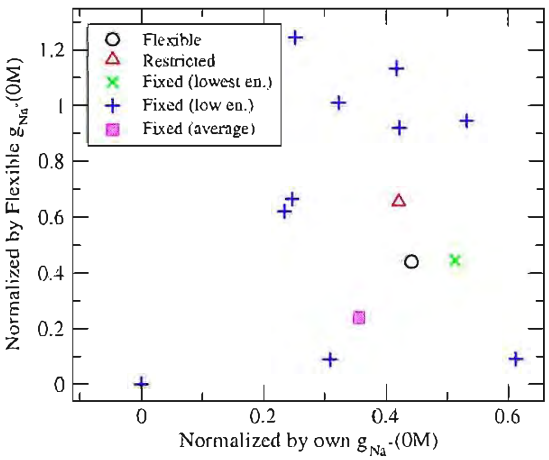

Figure 7. Correlation between Na^+ conductances normalized by two different ways for [$CaCl_2$] = 10^{-6} M. The ordinate shows the conductance of Na^+ normalized by the Na^+ conductance in the absence of Ca^{2+} for the 'flexible' case. The abscissa shows conductance of Na^+ for a given case normalized by the Na^+ conductance in the absence of Ca^{2+} for that particular case. Symbols have the same meaning as in figure 6.

regime, our agreement with experiments is only qualitative due to differences between the theoretical and experimental situations as described previously [76]. (In experiments, Ca^{2+} is added only to the extracellular side, while our setup is symmetrical.) Note that the occupancy and conductance curves for Na^+ behave similarly indicating a strong correlation between these two quantities (see the Discussion section).

Figure 6 shows the correlation between Na^+ conductance and Na^+ occupancy. The correlation was evident from figure 5, but this figure shows it clearly: the more Na^+ we have in the filter, the larger the pore's conductance for Na^+. Again, the various '*fixed*' oxygen points scatter over a relatively wide range, but this figure clearly shows that the large drop in both occupancy and conductance occurs in a relatively narrow concentration range around 1 μM. In the range of lower and higher [$CaCl_2$] (below and above 10^{-6} M), the values do not change very much. Also, the average of the ten '*low energy fixed*' cases is quite close the '*flexible*' and '*restricted*' cases that allow (some) movement of the oxygens.

In the previous figures, conductances were normalized by the conductances obtained at zero Ca^{2+} for a given case. Figure 7 was designed to show correlation between the conductances normalized in the two different ways described previously, if correlations existed. No correlations were found. Normalization of results from a model by the zero Ca^{2+} conductance of that model shows the selectivity of that model. The lower this normalized value (shown on the abscissa), the more selective the model is for Ca^{2+}. On the other hand, if we normalize by one specific value—the zero Ca^{2+} conductance for the '*flexible*' case—we can tell how the conductance of the model for Na^+ changes as we change the flexibility of the oxygen ions. The lack of correlation indicates that a given *fixed* oxygen configuration can favor selectivity and

conductance independently. Conductance is sensitive to the presence of depletion zones, while selectivity is more sensitive to the degree of competition between Ca^{2+} and Na^{+}.

The relative conductance in comparisons between different models depends primarily on the oxygen configuration. A configuration can be 'fortunate' (large conductance) so that Na^{+} ions find enough space between the crowding oxygen ions. A configuration could also be 'unfortunate', meaning that the oxygen ions are in positions that act as obstacles for the passing Na^{+} ions and produce deep depletion zones for them. Indeed, sometimes the location of oxygens creates depletion zones where Na^{+} concentration is zero, so the conductance is also zero. The '*flexible*' and '*restricted*' cases are statistical averages of the many '*fixed*' configurations in some sense or other. Therefore, these averaged cases do not suffer from the unfortunate configurations found in individual unaveraged cases: there are always enough configurations in the sample in the averaged cases in which oxygen ions move away and give way to the Na^{+} ions. The average of the ten '*low energy fixed*' cases is another example where the fortunate cases balance the unfortunate cases. Another interesting result shown in the figure is that the conductance of the '*restricted*' model is larger than that of the '*flexible*' model. The conductance is larger because the distribution of Na^{+} ions is more spatially uniform for this model (see figure 2). Therefore, the depletion zones of Na^{+} are less deep in this case.

Figure 8 shows the concentration profiles for $O^{-1/2}$, Na^{+}, and Ca^{2+} for our other model with different oxygen flexibility. When the oxygen ions are fixed ($R_{ox} = 0$ Å), the Na^{+} and Ca^{2+} ions have high peaks in the regions where oxygen ions are absent. As the R_{ox} is increased, the peaks become lower, the valleys become less deep, and the curves eventually converge to those of the '*flexible*' model.

Figure 9 shows the conductance and occupancy of Na^{+} as a function of R_{ox}. The conductances are normalized by the value at $R_{ox} = 0$ Å. There are two maxima in the conductance. It seems that conductance is larger in a model that is not perfectly '*flexible*', but not perfectly '*fixed*' either. In the '*fixed*' model, the oxygen ions act as obstacles as described above, especially if their configuration is 'unlucky'. In the '*flexible*' case, the oxygen ions act as obstacles because they pile up at the filter entrances thus producing depletion zones for the Na^{+} ions.

There is a clear correlation between conductance and occupancy: less Na^{+} means more Na^{+} conductance. Intuitively, we might expect the opposite. The explanation is that although we have less Na^{+} (smaller peaks), as R_{ox} is increased, we also—in the same profile—have shallower depletion zones (see figure 8).

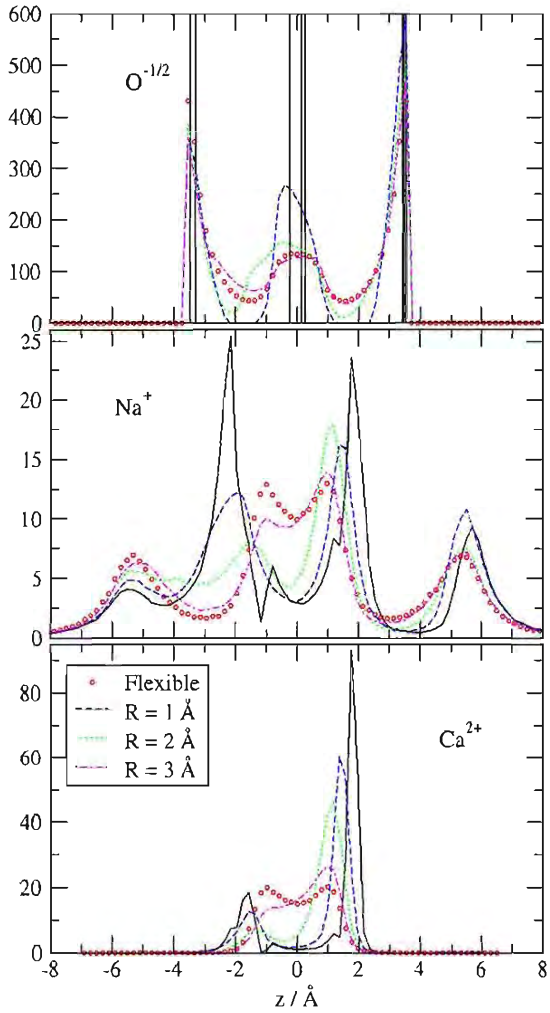

Figure 8. Concentration profiles of $O^{-1/2}$, Na^{+}, and Ca^{2+} for the 'flexible' (red circles) and the lowest-energy 'fixed' (solid black line) cases, as well as cases when the oxygens are restricted in spheres of radii R_{ox} centered around the 'fixed' positions (various colored non-solid curves) at $[CaCl_2] = 10^{-6}$ M.

4. Discussion

4.1. Some flexibility of side chains is required for calcium selectivity

We investigated the role of flexibility by comparing differential quantities and integral quantities in the selectivity filter of the 'flexible', 'fixed' and 'restricted' models. We compared the differential quantities, the distribution of the side chains (oxygens) and the cations (Na^{+} and Ca^{2+}) and the integrated quantities, the occupancies of cations Ca^{2+}/Na^{+} and linearized conductance of Na^{+}.

The differential quantities that we obtain from our model show a strong dependence on the locations of fixed side chains and the flexibility of the side chains. We show that holding the side chains fixed at certain predetermined locations in the selectivity filter distorts the distribution of Ca^{2+} and Na^{+} in the selectivity filter. This distortion can result in a loss in selectivity because the distribution of the cations is determined by the distribution of the side chains (figure 3(*C*)). This reasoning is further supported (1) by calculations (figure 8) which vary the mobility of the side chains in the radial direction from frozen to perfectly mobile and (2) by calculations (figures 3(*A*) and (*B*)) of the 'restricted model' in which the side chains are allowed

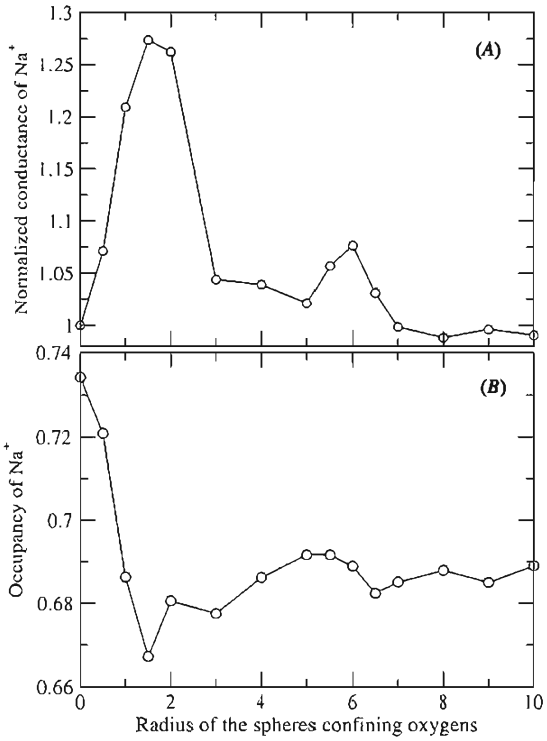

Figure 9. (*A*) Normalized conductance and (*B*) occupancy of Na^+ ions as functions of the spheres confining the oxygens R_{ox} for $[CaCl_2] = 10^{-6}$ M. The conductance is normalized by the 'fixed' ($R_{ox} = 0$ Å) case.

to have a limited flexibility along the channel axis. The results are similar to the usual 'flexible' case.

However, the behavior described by the integrated quantities (occupancy and normalized conductance) is much less sensitive, as might be expected from averaged, i.e. integrated quantities which are, as a rule, much less sensitive than differential quantities. Behavior of integrated quantities is similar in the 'restricted', 'fixed', and 'flexible' models. The occupancy of Ca^{2+} increases with increasing bath concentration of Ca^{2+} (while occupancy of Na^+ decreasing) and the normalized conductance of Na^+ is reduced with increasing amount of Ca^{2+} in bath. Thus, the integrated quantities obtained from our model are much less sensitive to details of structure. They do not show sensitivity to the flexibility and the locations of the side chains.

Our results show that some flexibility of side chains is necessary to avoid obstruction of the ionic pathway by oxygen ions in 'unlucky' fixed positions. When oxygen ions are mobile, they adjust 'automatically' to accommodate to the permeable cations in the selectivity filter.

Beyond the rigid (fixed oxygen) case, however, our results seem quite insensitive to how and what degree do we make the side chains flexible. Density profiles and selectivity (expressed in term of either occupancy or conductance) behave similarly in the different models of flexibility ('flexible', 'restricted', and 'confined').

The exact location and mobility of oxygen ions (let alone even finer details of structure) have little effect on the selectivity behavior of calcium channels. Seemingly, nature has chosen a robust mechanism to control selectivity in calcium channels: the first-order determinant of selectivity is the volume of the selectivity filter with the charge and excluded volume of structural ions confined within it. Flexibility of side chains seems to belong to the group of second-order determinants. These conclusions of course apply to what we study here. Flexibility and fine structural details may have important role in other properties of calcium channels that are not studied in this paper.

These results justify our early assumption—suggested by Nonner *et al* [55] using theory and further studied with MC simulations [54, 66, 104]—that the important factor in Ca^{2+} versus Na^+ selectivity is the density of oxygen ions in the selectivity filter. Later studies (41, 42) showed the importance of (charge) polarization (i.e. dielectric properties). The assumption of maximum mobility of oxygens ('flexible' case) seems to be an excellent approximate working hypothesis in the absence of exact structural information. We look forward to seeing how well the real structure fits within this hypothesis, when it becomes available.

4.2. *Self-organized induced-fit model of selectivity*

Our results from the simulations of the zero flexibility model and the restricted flexibility model suggest that the reduced model is actually an induced-fit model of selectivity, a specific version of the induced-fit model of enzymes [105] in which biological function is controlled by the flexibility of the side chains that allows the side chains to self-organize into structures that change with changing ionic conditions.

The variation of binding with concentration and type of ions arises from different structures that self-organize under different ionic conditions. The fit of the protein side chains to the ions, and the fit of the ions to the protein, change with conditions. The different fit in different types of ions produces selectivity. The structures—in the sense defined in this paper—vary with concentration as well as type of ion. The energy of the structures varies with concentration and type of ion and we know of no simple theory to calculate this change in energy. Simulations are needed in a range of concentrations and types of solutions. Calculations that characterize selectivity by a single free energy of binding do not address these issues. They also do not address the issue of how selectivity occurs in life or in experiments in which ions appear in mixed solutions of varying concentrations.

Induced-fit and self-organized models have traditionally been focused on the average structure of the protein. Here we view the locations of ions as part of the structure and we find that the distribution of locations ('flexibility', 'entropy') is also important. MC methods used by Boda *et al* [69, 70, 76, 104, 106, 107] seem ideally suited to make the qualitative idea of self-organized systems and induced fit of enzymes into a quantitatively specific (and testable) hypothesis of protein function. The self-organized/induced-fit theory states that all relevant atoms are in an equilibrium distribution of positions and (perhaps) velocities. MC methods are used to estimate such distributions in many areas of physics. These methods

seem to be less sensitive to sampling errors than traditional forms of molecular dynamics for many reasons discussed at length in the literature [108, 109].

Selectivity in these channels arises from the interaction of the flexible side chains with the ions. The balance of the two main competing forces—electrostatic and excluded volume—in the crowded selectivity filter of the reduced model determines the binding site for Ca^{2+}. The structure of the binding site is an output of the calculations which rearranges according to the surrounding ionic conditions. The word 'structure' is somewhat inadequate to describe what is happening here. The thermal motions of the structure are as important as the average location. The biologically important properties depend on the entire ensemble of trajectories of ions and side chains. The distributions of location and velocities are involved. Traditional self-organized/induced-fit models need to be generalized to include the self-organized/induced entropy (i.e., flexibility) as well as the self-organized/induced energy (i.e. location).

The success of the self-organized induced-fit model of selectivity arises because it calculates structures instead of assuming them. Assuming a preformed structure, independent of conditions, distorts the model significantly. Evidently, assuming a constant structure involves applying an artificial constraint not present in real channels. We suspect, but have not proven, that the difficulty is fundamentally similar to that which arises when a protein is described by a potential surface independent of conditions instead of as a distribution of permanent and dielectric charge [86, 87].

MC methods developed by Boda *et al* seem ideally suited to compute the equilibrium properties of these self-organized systems. Other methods are needed to extend to the general non-equilibrium conditions in which most channels and proteins function, for example, variational methods like the Energy Variational Approach (EnVarA) [50, 51] or Poisson-Nernst-Planck/Density Functional Theory (PNP-DFT) [98, 102, 103].

Acknowledgments

We thank our colleague and friend Professor Eduardo Rios for suggesting the name '*flexible confinement*'. We are grateful for a generous allotment of computing time at the MARYLOU supercomputing facility of Brigham Young University. Discussions with Wolfgang Nonner and Dirk Gillespie were most valuable and welcome. The work was supported in part by NIH grant GM076013. DB acknowledges the support of the Hungarian National Research Fund (OTKA K75132).

References

[1] Roux B 2010 Perspectives on: molecular dynamics and computational methods *J. Gen. Physiol.* **135** 547–8
[2] Roux B 2010 Exploring the ion selectivity properties of a large number of simplified binding site models *Biophys. J.* **98** 2877–85
[3] Hagiwara S and Naka K I 1964 The initiation of spike potential in barnacle muscle fibers under low intracellular Ca^{++} *J. Gen. Physiol.* **48** 141–62
[4] Gerasimov V D, Kostyuk P G and Maiskii V A 1965 Action potential production in giant neurons of mollusks *Fed. Proc. Transl. Suppl.* **24** (5) 763–7
[5] Kostyuk P G, Krishtal O A, Pidoplichko V I and Veselovsky N S 1978 Ionic currents in the neuroblastoma cell membrane *Neuroscience* **3** 327–32
[6] Hagiwara S 1979 Differentiation of Na and Ca channels during early development *Soc. Gen. Physiol. Ser.* **33** 189–97
[7] Byerly L and Hagiwara S 1982 Calcium currents in internally perfused nerve cell bodies of *Limnea stagnalis J. Physiol.* **322** 503–28
[8] Hagiwara S and Ohmori H 1982 Studies of calcium channels in rat clonal pituitary cells with patch electrode voltage clamp *J. Physiol.* **331** 231–52
[9] Almers W and McCleskey E W 1984 Non-selective conductance in calcium channels of frog muscle: calcium selectivity in a single-file pore *J. Physiol.* **353** 585–608
[10] Hagiwara S and Kawa K 1984 Calcium and potassium currents in spermatogenic cells dissociated from rat seminiferous tubules *J. Physiol.* **356** 135–49
[11] Lee K S and Tsien R W 1984 High selectivity of calcium channels in single dialyzed heart cells of the guinea pig *J. Physiol.* **354** 253–72
[12] Tsien R W, Hess P, McCleskey E W and Rosenberg R L 1987 Calcium channels: mechanisms of selectivity, permeation, and block *Annu. Rev. Biophys. Biophys. Chem.* **16** 265–90
[13] Kostyuk P G 1989 Diversity of calcium ion channels in cellular membranes *Neuroscience* **28** 253–61
[14] Corvalan V, Cole R, de Vellis J and Hagiwara S 1990 Neuronal modulation of calcium channel activity *in* cultured rat astrocytes *Proc. Natl Acad. Sci. USA* **87** 4345–8
[15] Yamashita N, Ciani S and Hagiwara S 1990 Effects of internal Na^+ on the Ca channel outward current in mouse neoplastic B lymphocytes *J. Gen. Physiol.* **96** 559–79
[16] Kostyuk P and Verkhratsky A 1994 Calcium stores in neurons and glia *Neuroscience* **63** 381–404
[17] McCleskey E W 1994 Calcium channels: cellular roles and molecular mechanisms *Curr. Opin. Neurobiol.* **4** 304–12
[18] Kirischuk S, Voitenko N, Kostyuk P and Verkhratsky A 1996 Calcium signalling in granule neurones studied in cerebellar slices *Cell Calcium* **19** 59–71
[19] Zhang J F, Ellinor P T, Aldrich R W and Tsien R W 1996 Multiple structural elements in voltage-dependent Ca^{2+} channels support their inhibition by G proteins *Neuron* **17** 991–1003
[20] Rodríguez-Contreras A and Yamoah E N 2003 Effects of permeant ion concentrations on the gating of L-type Ca^{2+} channels in hair cells *Biophys. J.* **84** 3457–69
[21] Gordon S E 2010 Perspectives on: local calcium signaling *J. Gen. Physiol.* **136** 117
[22] Boda D, Nonner W, Valiskó M, Henderson D, Eisenberg B and Gillespie D 2007 Steric selectivity in Na channels arising from protein polarization and mobile side chains *Biophys. J.* **93** 1960–80
[23] Boda D, Valiskó M, Henderson D, Eisenberg B, Gillespie D and Nonner W 2009 Ionic selectivity in L-type calcium channels by electrostatics and hard-core repulsion *J. Gen. Physiol.* **133** 497–509
[24] Rahin A A and Honig B 1985 Reevaluation of the Born model of ion hydration *J. Phys. Chem.* B **89** 5588–93
[25] Gilson M K and Honig B 1985 The dielectric constant of a folded protein *Biopolymers* **25** 2097–119
[26] Warshel A and Russell S T 1984 Calculations of electrostatic interactions in biological systems and in solutions *Q. Rev. Biophys.* **17** 283–422
[27] Russell S T and Warshel A 1985 Calculations of electrostatic energies in proteins. The energetics of ionized groups in bovine pancreatic trypsin inhibitor *J. Mol. Biol.* **185** 389–404

[28] Head-Gordon T and Brooks C L 1987 The role of electostatics in the binding of small ligands to enzymes *J. Phys. Chem.* B **91** 3342–9

[29] Gilson M K and Honig B 1988 Calculation of the total electrostatic energy of a macromolecular system: solvation energies, binding energies, and conformational analysis *Proteins* **4** 7–18

[30] Gilson M K, Sharp K A and Honig B H 1988 Calculating the electrostatic potential of molecules in solution: method and error assessment *J. Comput. Chem.* **9** 327–35

[31] Honig B, Sharp K and Gilson M 1989 Electrostatic interactions in proteins *Computer Assisted Modeling of Receptor-Ligand Interactions: Theoretical Aspects and Applications to DNA Design* ed R Rein and A Golombek (New York: Alan R Liss) pp 65–74

[32] Davis M E and McCammon J A 1990 Electrostatics in biomolecular structure and dynamics *Chem. Rev.* **90** 509–21

[33] Sharp K, Jean- Charles A and Honig B 1992 A local dilectric constant model for solvation free energies which accounts for solute polarizability *J. Phys. Chem.* B **96** 3822–8

[34] Honig B and Sharp K 1993 Macroscopic models of aqueous solutions: biological and chemical applications *J. Phys. Chem.* **97** 1101–9

[35] Gilson M K 1995 Theory of electrostatic interactions in macromolecules *Curr. Opin. Struct. Biol.* **5** 216–23

[36] Honig B and Nichols A 1995 Classical electrostatics in biology and chemistry *Science* **268** 1144–9

[37] Antosiewicz J, McCammon J A and Gilson M K 1996 The determinants of pKas in proteins *Biochemistry* **35** 7819–33

[38] Simonson T and Brooks C L 1996 Charge screening and the dielectric constant of proteins: insights from molecular dynamics *J. Am. Chem. Soc.* **118** 8452–8

[39] Warshel A 1998 Electrostatic origin of the catalytic power of enzymes and the role of preorganized active sites *J. Biol. Chem.* **273** 27035–8

[40] Dominy B N and Brooks C L 1999 Development of generalized Born model parameterization for proteins and nucleic acids *J. Phys. Chem.* B **103** 3675–773

[41] Roux B 2001 Implicit solvent models *Computational Biochemistry and Biophysics* ed O Becker, A D MacKerrel, B Roux and M Watanabe (New York: Dekker)

[42] Schutz C N and Warshel A 2001 What are the dielectric 'constants' of proteins and how to validate electrostatic models? *Proteins* **44** 400–17

[43] Baker N A and McCammon J A 2005 Electrostatic interactions *Structural Bioinformatics* ed H Weissig and P E Bourne (New York: Wiley)

[44] Im W, Lee M S and Brooks C L III 2003 Generalized Born model with a simple smoothing function *J. Comput. Chem.* **24** (14) 1691–702

[45] Nielsen J E and McCammon J A 2003 Calculating pKa values in enzyme active sites *Protein Sci.* **12** 1894–901

[46] Swanson J M, Mongan J and McCammon J A 2005 Limitations of atom-centered dielectric functions in implicit solvent models *J. Phys. Chem.* B **109** 14769–72

[47] Zhu J, Alexov E and Honig B 2005 Comparative study of generalized Born models: Born raddi and peptide folding *J. Phys. Chem.* B **109** 3008–22

[48] Dzubiella J, Swanson J M and McCammon J A 2006 Coupling hydrophobicity, dispersion, and electrostatics in continuum solvent models *Phys. Rev. Lett.* **96** 087802

[49] Henderson D 2009 Attractive energy and entropy or particle size: the Yin and Yang of physical and biological science *Interdiscip. Sci.: Comput. Life Sci.* **1** 1–11

[50] Hyon Y, Eisenberg B and Liu C 2010 A mathematical model for the hard sphere repulsion in ionic solutions *Comm. Math. Sci.* at press, also available as preprint# 2318 (IMA, University of Minnesota, Minneapolis) http://www.ima.umn.edu/preprints/jun2010/jun2010.html

[51] Eisenberg B, Hyon Y and Liu C 2010 Energy variational analysis EnVarA of ions in water and channels: field theory for primitive models of complex ionic fluids *J. Chem. Phys.* **133** 104104

[52] Barreiro G, Guimaraes C R and de Alencastro R B 2002 A molecular dynamics study of an L-type calcium channel model *Protein Eng.* **15** (2) 109–22

[53] Lipkind G M and Fozzard H A 2001 Modeling of the outer vestibule and selectivity filter of the L-type Ca^{2+} channel *Biochemistry* **40** 6786–94

[54] Malasics A, Gillespie D, Nonner W, Henderson D, Eisenberg B and Boda D 2009 Protein structure and ionic selectivity in calcium channels: selectivity filter size, not shape, matters *Biochim. Biophys. Acta* **1788** 2471–80

[55] Nonner W, Catacuzzeno L and Eisenberg B 2000 Binding and selectivity in L-type Ca channels: a mean spherical approximation *Biophys. J.* **79** 1976–92

[56] Rutkai G, Boda D and Kristóf T 2010 Relating binding affinity to dynamical selectivity from dynamic Monte Carlo simulations of a model calcium channel *J. Phys. Chem. Lett.* **1** 2179–84

[57] Markowich P A, Ringhofer C A and Schmeiser C 1990 *Semiconductor Equations* (New York: Springer-Verlag)

[58] Shur M 1990 *Physics of Semiconductor Devices* (New York: Prentice-Hall)

[59] Eisenberg B 2005 Living transistors: a physicist's view of ion channels (version 2) arXiv:q-bio/0506016v2

[60] Yang J, Ellinor P T, Sather W A, Zhang J F and Tsien R 1993 Molecular determinants of Ca^{2+} selectivity and ion permeation in L-type Ca^{2+} channels *Nature* **366** 158–61

[61] Ellinor P T, Yang J, Sather W A, Zhang J-F and Tsien R 1995 Ca^{2+} channel selectivity at a single locus for high-affinity Ca^{2+} interactions *Neuron* **15** 1121–32

[62] Wu X S, Edwards H D and Sather W A 2000 Side chain orientation in the selectivity filter of a voltage-gated Ca^{2+} channel *J. Biol. Chem.* **275** 31778–85

[63] Sather W A and McCleskey E W 2003 Permeation and selectivity in calcium channels *Annu. Rev. Physiol.* **65** 133–59

[64] Koch S E, Bodi I, Schwartz A and Varadi G 2000 Architecture of Ca^{2+} channel pore-lining segments revealed by covalent modification of substituted cysteines *J. Biol. Chem.* **275** 34493–500

[65] McCleskey E W 2000 Ion channel selectivity using an electric stew *Biophys. J.* **79** 1691–2

[66] Boda D, Valiskó M, Eisenberg B, Nonner W, Henderson D and Gillespie D 2007 Combined effect of pore radius and protein dielectric coefficient on the selectivity of a calcium channel *Phys. Rev. Lett.* **98** 168102

[67] Boda D, Valiskó M, Eisenberg B, Nonner W, Henderson D and Gillespie D 2006 The effect of protein dielectric coefficient on the ionic selectivity of a calcium channel *J. Chem. Phys.* **125** 34901

[68] Valleau J P and Cohen L K 1980 Primitive model electrolytes: I. Grand canonical Monte Carlo computations *J. Chem. Phys.* **72** 5935–41

[69] Boda D, Henderson D and Busath D 2002 Monte Carlo study of the selectivity of calcium channels: improved geometrical mode *Mol. Phys.* **100** 2361–8

[70] Boda D, Nonner W, Henderson D, Eisenberg B and Gillespie D 2008 Volume exclusion in calcium selective channels *Biophys. J.* **94** 3486–96

[71] Malasics A, Gillespie D and Boda D 2008 Simulating prescribed particle densities in the grand canonical ensemble using iterative algorithms *J. Chem. Phys.* **128** 124102

[72] Malasics A and Boda D 2010 An efficient iterative grand canonical Monte Carlo algorithm to determine individual ionic chemical potentials in electrolytes *J. Chem. Phys.* **132** 244103

[73] Boda D, Gillespie D, Nonner W, Henderson D and Eisenberg B 2004 Computing induced charges in inhomogeneous dielectric media: application in a Monte Carlo simulation of complex ionic systems *Phys. Rev.* E **69** 046702

[74] Almers W, McCleskey E W and Palade P T 1984 Non-selective cation conductance in frog muscle membrane blocked by micromolar external calcium ions *J. Physiol.* **353** 565–83

[75] Nonner W and Eisenberg B 1998 Ion permeation and glutamate residues linked by Poisson–Nernst–Planck theory in L-type calcium channels *Biophys. J.* **75** 1287–305

[76] Gillespie D and Boda D 2008 The anomalous mole fraction effect in calcium channels: a measure of preferential selectivity *Biophys. J.* **95** 2658–72

[77] Varma S, Sabo D and Rempe S B 2008 K^+/Na^+ selectivity in K channels and valinomycin: over-coordination versus cavity-size constraints *J. Mol. Biol.* **376** 13–22

[78] Hille B 1975 Ionic selectivity, saturation, and block in sodium channels. A four barrier model *J. Gen. Physiol.* **66** 535–60

[79] Hille B 2001 *Ionic Channels of Excitable Membranes* (Sunderland, MA: Sinauer Associates)

[80] Cooper K, Jakobsson E and Wolynes P 1985 The theory of ion transport through membrane channels *Prog. Biophys. Mol. Biol.* **46** 51–96

[81] Hänggi P, Talkner P and Borokovec M 1990 Reaction-rate theory: fifty years after Kramers *Rev. Mod. Phys.* **62** 251–341

[82] Fleming G and Hänggi P 1993 *Activated Barrier Crossing: Applications in Physics, Chemistry and Biology* (River Edge, NJ: World Scientific)

[83] Cooper K E, Gates P Y and Eisenberg R S 1988 Surmounting barriers in ionic channels *Q. Rev. Biophys.* **21** 331–64

[84] Cooper K E, Gates P Y and Eisenberg R S 1988 Diffusion theory and discrete rate constants in ion permeation *J. Membr. Biol.* **106** 95–105

[85] Eisenberg R S, Klosek M M and Schuss Z 1995 Diffusion as a chemical reaction: stochastic trajectories between fixed concentrations *J. Chem. Phys.* **102** 1767–80

[86] Eisenberg R S 1996 Computing the field in proteins and channels *J. Membr. Biol.* **150** 1–25 arXiv:1009.2857v1001

[87] Eisenberg R S 1996 Atomic biology, electrostatics and ionic channels *New Developments and Theoretical Studies of Proteins* ed R Elber (Philadelphia, PA: World Scientific) pp 269–357 arXiv:0807.0715

[88] Chen D, Xu L, Tripathy A, Meissner G and Eisenberg R 1997 Rate constants in channology *Biophys. J.* **73** 1349–54

[89] Eisenberg R S 1999 From structure to function in open ionic channels *J. Membr. Biol.* **171** 1–24

[90] Eisenberg B 2008 Permeation as a diffusion process arXiv:0807.0721

[91] Dang T X and McCleskey E W 1998 Ion channel selectivity through stepwise changes in binding affinity *J. Gen. Physiol.* **111** 185–93

[92] Wu XS Edward H D and Sather W A 2000 Side chain orientation in the selectivity filter of a voltage-gated Ca^{2+} channel *J. Biol.Chem.* **275** 31778–85

[93] Cibulsky S M and Sather W A 2000 The EEEE locus is the sole high-affinity Ca^{2+} binding structure in the pore of a voltage-gated Ca^{2+} channel: block by Ca^{2+} entering from the intracellular pore entrance *J. Gen. Physiol.* **116** 349–62

[94] Gubernatis J E (ed) 2003 *The Monte Carlo Method in the Physical Sciences (AIP Conference Proceedings* vol 690*)* (Melville, NY: American Institute of Physics)

[95] Christian P R and Casella G 2004 *Monte Carlo Statistical Methods (Springer Texts in Statistics)* 2nd edn (New York: Springer)

[96] Gillespie D, Boda D, He Y, Apel P and Siwy Z S 2008 Synthetic nanopores as a test case for ion channel theories: the anomalous mole fraction effect without single filing *Biophys. J.* **95** 609–19

[97] Gillespie D, Nonner W and Eisenberg R S 2002 Coupling Poisson–Nernst–Planck and density functional theory to calculate ion flux *J. Phys.: Condens. Matter.* **14** 12129–45

[98] Gillespie D 2008 Energetics of divalent selectivity in a calcium channel: the ryanodine receptor case study *Biophys. J.* **94** 1169–84

[99] Gillespie D, Giri J and Fill M 2009 Reinterpreting the anomalous mole fraction effect. The ryanodine receptor case study *Biophyiscal J.* **97** 2212–21

[100] Gillespie D 2010 Analytic theory for dilute colloids in a charged slit *J. Phys. Chem.* B **114** 4302–9

[101] Eisenberg B 2010 Crowded charges in ion channels *Adv. Chem. Phys.* at press arXiv:1009.1786v1

[102] Gillespie D, Valiskó M and Boda D 2005 Density functional theory of the electrical double layer: the RFD functional *J. Phys.: Condens. Matter.* **17** 6609–26

[103] Gillespie D, Xu L, Wang Y and Meissner G 2005 (De)construcing the ryanodine receptor: modeling ion permeation and selectivity of the calcium release channel *J. Phys. Chem.* **109** 15598–610

[104] Boda D, Henderson D and Busath D D 2001 Monte Carlo study of the effect of ion and channel size on the selectivity of a model calcium channel *J. Phys. Chem.* B **105** 11574–7

[105] Koshland D 1958 Application of a theory of enzyme specificity to protein synthesis *Proc. Natl Acad. Sci.* **44** 98–104

[106] Boda D, Busath D D, Henderson D and Sokolowski S 2000 Monte Carlo simulations of the mechanism of channel selectivity: the competition between volume exclusion and charge neutrality *J. Phys. Chem.* B **104** 8903–10

[107] Boda D, Busath D, Eisenberg B, Henderson D and Nonner W 2002 Monte Carlo simulations of ion selectivity in a biological Na^+ channel: charge-space competition *Phys. Chem. Chem. Phys. (PCCP)* **4** 5154–60

[108] Kokubo H, Rosgen J, Bolen D W and Pettitt B M 2007 Molecular basis of the apparent near ideality of urea solutions *Biophys. J.* **93** 3392–407

[109] Yu H and Roux B 2009 On the utilization of energy minimization to the study of ion selectivity *Biophys. J.* **97** L15–17